

On the Modeling of Miscible Flow in Multi-Component Porous Media

M. BAI¹ and D. ELSWORTH²

¹*School of Petroleum and Geological Engineering, University of Oklahoma, Norman, OK 73019–0628, U.S.A.*

²*Department of Mineral Engineering, Pennsylvania State University, University Park, PA 16802–5000, U.S.A.*

(Received: 24 October 1994; in final form: 11 April 1995)

Abstract. An analytical model of miscible flow in multi-component porous media is presented to demonstrate the influence of pore capacitance in extending diffusive tailing. Solute attenuation is represented naturally by accommodating diffusive and convective flux components in macropores and micropores as elicited by the local solute concentration and velocity fields. A set of twin, coupled differential equations result from the Laplace transform and are solved simultaneously using a differential operator for one-dimensional flow geometry. The solutions in real space are achieved using numeric inversion. In addition, to represent more faithfully the dominant physical processes, this approach enables efficient and stable semi-analytical solution procedure of the coupled system that is significantly more complex than current capacitance type models. Parametric studies are completed to illustrate the ability of the model to represent sharp breakthrough and lengthy tailing, as well as investigating the form of the nested heterogeneity as a result of solute exchange between macropores and micropores. Data from a laboratory column experiment is examined using the present model and satisfactory agreement results.

Key words: Miscible flow, micropore convection, micropore diffusion, heterogeneity, breakthrough curve.

0. Nomenclature

Roman Letters

- a* rate coefficient of internal flow
- b* velocity ratio (v_1/v_2)
- h* dispersion ratio (D_2/D_1)
- c_1 macropore concentration
- c_2 micropore concentration
- \bar{c}_1 macropore concentration in Laplace space
- \bar{c}_2 micropore concentration in Laplace space
- c_1^0 macropore concentration at source location
- c_2^0 micropore concentration at source location
- D_1 macropore dispersion coefficient
- D_2 micropore dispersion coefficient
- f* fraction of pore space occupied by fluid in primary channel
- L* length of laboratory sample column
- K* mass exchange rate
- t* time from initial stage
- v_1 primary flow channel velocity

v_2 micropore interstitial velocity
 x distance from source
 y dimensionless distance

Greek Letters

γ equivalent Péclet number
 τ dimensionless time, or injected pore volume

1. Introduction

For a homogeneous porous medium, miscible flow is usually defined in terms of a single fluid with the independent variable taken as the concentration. For multi-component media, where characteristic lengths are distinctly different between the flow-interacting units, two fluids remain separate and occupy their own volume, but fluids are interchangeable during the transport process due to their miscibility. It is generally recognized that heterogeneous porous media present capacitance effects during miscible displacement due to noninstantaneous equilibrium of concentration between mobile fluid in macropores and immobile fluid in micropores. The latter results from the stagnant fluid frequently isolated in dead-end pores. The geometric relationship between micropores and macropores is illustrated in Figure 1. Large open channels present in macropores comprise the primary flow pathways, with interstitial micropores acting as capacitors in storing or recharging the flow to the macropores, depending on the relative concentration gradient between the two component spaces.

The impact of heterogeneities at various scales precludes the use of the classical convection-dispersion approach because the transport process can not be represented by superposition of a simple diffusive process. Capacitance models have been applied to replicate the nonhomogeneous behavior observed in porous media exhibiting storage perturbation. Observation of abrupt solute breakthrough accompanied by extensive tailing is often attributed to the storage interchange between flowing liquid in macropores and stagnant fluid in micropores. (Deans, 1963; Coats and Smith, 1964; Passioura, 1971; Passioura and Rose, 1971; Piquemal, 1992, 1993). In addition to its utility in modeling tracer dispersion in naturally heterogeneous porous media, capacitance models has been used in the simulation of particle transport in partially clogged porous media where the heterogeneity may evolve with the progress of clogging. Consequently, local rectification of flow pathways corresponds to morphological and structural changes occurring in the clogged porous media (Bouhroum, 1993). Dual-porosity models provide a natural analog to capacitance models where fractures and matrix blocks are considered as interacting porous components. The rate of mass transfer depends on either the relative magnitude of concentration gradient, or the degree of permeability contrast between the two interacting media (Tang *et al.*, 1981; Bibby, 1981; Huyakorn *et al.*,

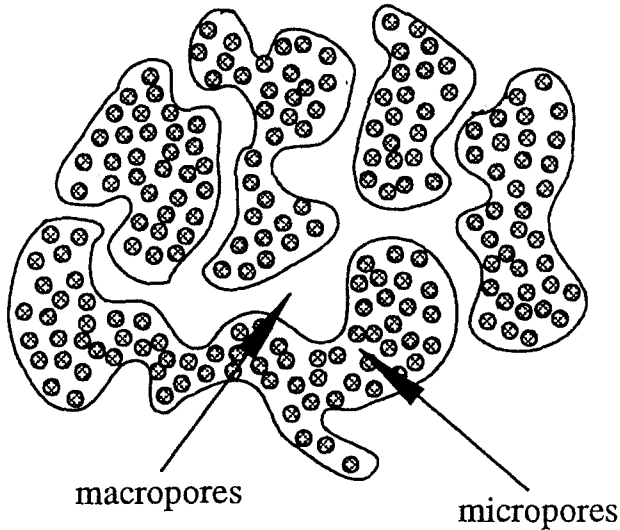


Fig. 1. Micropore-macropore media in capacitance model.

1983; Nilson and Lie, 1990; Rowe and Booker, 1990; Sudicky and McLaren, 1992; Harrison *et al.*, 1992; Leo and Booker, 1993).

Despite the wide utilization of the capacitance concept, these models provide poor representation of the extended tailing phenomenon observed in moderately and highly heterogeneous porous media (Joy and Kouwen, 1991; Imdakm and Sahimi, 1991; Koenders and Williams, 1992; Joy *et al.*, 1993). The lack of a physical basis in supporting the capacitance model was noted by Bouhroum (1993) in reference to experimental results. Bouhroum (1993) showed that the early solute penetration and long tailing of breakthrough curves were the result of velocity fluctuations induced by layers of different permeability and particle clogging, respectively. The existence of low permeability zones delays the rate of solute transport while simultaneously increasing the skewness of the breakthrough curves. Although these experimental results were adequately approximated by capacitance models through manipulation of input parameters, the fidelity of the match was more a result of the curve-fitting procedure rather than an adequate physical replication of actual transport processes. One undesirable feature of capacitance approaches rests on its physically spurious assumption that there is no flow within the micropore space. In reality, flow in the micropores should be either diffusive at low flow velocities or convective at high local velocities. Under more significant concentration gradients and at higher local flow velocities, both diffusion and convection need be included in representing transport in micropores. As pointed out by Udey and Spanos (1993) in the construction of a mathematical model for miscible flow in nonhomogeneous media, the two sets of equations (one representing macropores and another representing micropores) should be identical. In other words, the effects of diffusion (dispersion) and convection should be maintained for both macropore and micro-

pore spaces. The incorporation of micro-convection and micro-diffusion in the formulation of an alternative capacitance model constitutes the primary objective of the following work.

2. Analytical Formulation and Solutions

The capacitance model developed by Coats and Smith (1964) can be equivalently expressed as

$$D_1 \frac{\partial^2 c_1}{\partial x^2} - v_1 \frac{\partial c_1}{\partial x} = f \frac{\partial c_1}{\partial t} + K(c_1 - c_2), \quad (1)$$

$$0 = (1 - f) \frac{\partial c_2}{\partial t} - K(c_1 - c_2), \quad (2)$$

where c_1 and c_2 are the solute concentrations for macropores and micropores, respectively; D_1 is the macropore dispersion coefficient, v_1 is the average velocity in primary flow channel, f is the fraction of pore space occupied by mobile fluid, K is the rate of mass exchange between macropores and micropores, x is the distance from source, and t is the time. The zero on the left hand side of Equation (2) implies that liquid in the micropores is stagnant.

Considering the dispersive as well as convective flow processes within the micropores, two terms should be used to substitute the zero on the left-hand side of Equation (2). Therefore

$$D_2 \frac{\partial^2 c_2}{\partial x^2} - v_2 \frac{\partial c_2}{\partial x} = (1 - f) \frac{\partial c_2}{\partial t} - K(c_1 - c_2), \quad (3)$$

where D_2 is the micropore dispersion coefficient, and v_2 is the micropore interstitial velocity.

Equations (1) and (3) represent the governing equations of solute transport in porous media incorporating micropore dispersion and convection. It is more convenient to utilize dimensionless variables in the formulation by replacing the dimensional variables:

$$\begin{aligned} b &= \frac{v_1}{v_2}, & h &= \frac{D_2}{D_1}, \\ y &= \frac{x}{L}, & \tau &= \frac{v_1 t}{L}, \\ \gamma &= \frac{v_1 L}{D_2}, & a &= \frac{K L}{v_1}, \end{aligned} \quad (4)$$

where b is the coefficient representing the proportionality between flow velocities in macropores and micropores, h is the ratio of dispersion coefficients between micropores and macropores, L is an arbitrary length representing the longest possible

solute travel distance, y is the dimensionless distance, τ is the dimensionless time or injected pore volume, γ is the equivalent Peclet number considering the ratio between macropore velocity and micropore dispersion, and a is the rate coefficient of internal flow.

In dimensionless form, Equation (1) and (3) may be written as

$$\frac{1}{h\gamma} \frac{\partial^2 c_1}{\partial y^2} - \frac{\partial c_1}{\partial y} = f \frac{\partial c_1}{\partial \tau} + a(c_1 - c_2), \quad (5)$$

$$\frac{1}{\gamma} \frac{\partial^2 c_2}{\partial y^2} - \frac{1}{b} \frac{\partial c_2}{\partial y} = (1 - f) \frac{\partial c_2}{\partial \tau} - a(c_1 - c_2). \quad (6)$$

For application of a step change in solute concentration at one end and no variation in solute flux at the other end, the boundary and initial conditions may be defined as

$$\begin{aligned} c_1 &= c_1^0, c_2 = c_2^0 \quad (y = 0), \\ \frac{\partial c_1}{\partial y} &= \frac{\partial c_2}{\partial y} = 0 \quad (y = 1), \\ c_1 &= c_2 = 0 \quad (t = 0), \end{aligned} \quad (7)$$

where c_1^0 and c_2^0 are the macropore and micropore concentration at source location, respectively.

Using the Laplace transform, Equations (5) and (6) can be modified into ordinary differential equations and the time dependence removed as

$$\frac{1}{h\gamma} \frac{d^2 \bar{c}_1}{dy^2} - \frac{d\bar{c}_1}{dy} = f s \bar{c}_1 + a(\bar{c}_1 - \bar{c}_2), \quad (8)$$

$$\frac{1}{\gamma} \frac{d^2 \bar{c}_2}{dy^2} - \frac{1}{b} \frac{d\bar{c}_2}{dy} = (1 - f) s \bar{c}_2 - a(\bar{c}_1 - \bar{c}_2). \quad (9)$$

The boundary conditions in the Laplace domain are given as

$$\begin{aligned} \bar{c}_1 &= \frac{\bar{c}_1^0}{s}, \quad \bar{c}_2 = \frac{\bar{c}_2^0}{s} \quad (y = 0), \\ \frac{d\bar{c}_1}{dy} &= \frac{d\bar{c}_2}{dy} = 0 \quad (y = 1). \end{aligned} \quad (10)$$

The method of differential operators (*Mathematical Handbook*, 1979) is applied in this work to accommodate the coupled behavior of Equations (8) and (9). The differential operators, D^n , is applied as

$$D^n f(x_i) = \frac{d^n f(x_i)}{dx_i^n}, \quad (11)$$

where i indexes an arbitrary variable, and n is the order of the differential equations.

Applying the differential operators to Equations (8) and (9), gives

$$\left(\frac{D^2}{h\gamma} - D - \beta_2\right) \bar{c}_1 + a\bar{c}_2 = 0, \quad (12)$$

$$\left[\frac{D^2}{\gamma} - \frac{D}{b} + \beta_1\right] \bar{c}_2 + a\bar{c}_1 = 0, \quad (13)$$

where

$$\beta_1 = -[a + (1 - f)s], \quad \beta_2 = a + fs. \quad (14)$$

Solving Equations (12) and (13) simultaneously, yields

$$\bar{c}_1 = \frac{-1}{a} \left[\frac{D^2}{\gamma} - \frac{D}{b} + \beta_1\right] \bar{c}_2. \quad (15)$$

Substituting Equation (15) into (12) results in

$$(D^4 + B_1D^3 + B_2D^2 + B_3D + B_4)\bar{c}_2 = 0, \quad (16)$$

where

$$\begin{aligned} B_1 &= -\gamma \left(h + \frac{1}{b}\right), & B_2 &= h\gamma \left(\frac{\beta_1}{h} + \frac{\gamma}{b} - \beta_2\right), \\ B_3 &= h\gamma^2 \left(\frac{\beta_2}{b} - \beta_1\right), & B_4 &= -h\gamma^2(\beta_1\beta_2 + a^2). \end{aligned} \quad (17)$$

Equation (16) has four roots from the following equations (*Mathematical Handbook*, 1979):

$$D^2 + \xi_1 D + \phi_1 = 0, \quad (18)$$

$$D^2 + \xi_2 D + \phi_2 = 0, \quad (19)$$

where

$$\begin{aligned} \Delta_1 &= 8z + B_1^2 - 4B_2, \\ \xi_1 &= 0.5(B_1 + \sqrt{\Delta_1}), & \xi_2 &= 0.5(B_1 - \sqrt{\Delta_1}), \\ \phi_1 &= z + \frac{B_1 z - B_3}{\sqrt{\Delta_1}}, & \phi_2 &= z - \frac{B_1 z - B_3}{\sqrt{\Delta_1}}, \end{aligned} \quad (20)$$

where z is any real root of the following equation:

$$8z^3 + 4E_1z^2 + E_2z + E_3 = 0, \quad (21)$$

and where

$$\begin{aligned} E_1 &= -B_2, \\ E_2 &= 2B_1B_3 - 8B_4, \\ E_3 &= B_4(4B_2 - B_1^2) - B_3^2. \end{aligned} \quad (22)$$

Further, assume

$$z = u - \frac{E_1}{6}, \quad (23)$$

where the parameter u can be determined from the third-order equation

$$u^3 + pu + q = 0, \quad (24)$$

and where

$$\begin{aligned} p &= 0.125 \left(E_2 - \frac{2E_1^2}{3} \right), \\ q &= 0.125 \left(\frac{2E_1^3}{27} - \frac{E_1E_2}{6} + E_3 \right). \end{aligned} \quad (25)$$

The three roots of u may be described as

$$\begin{aligned} u_1 &= F_1 + F_2, \\ u_2 &= \omega_1 F_1 + \omega_2 F_2, \\ u_3 &= \omega_2 F_1 + \omega_1 F_2, \end{aligned} \quad (26)$$

where

$$\begin{aligned} \Delta^* &= \left(\frac{q}{2} \right)^2 + \left(\frac{p}{3} \right)^3, \\ F_1 &= \left(-\frac{q}{2} + \sqrt{\Delta^*} \right)^{\frac{1}{3}}, \quad F_2 = \left(-\frac{q}{2} - \sqrt{\Delta^*} \right)^{\frac{1}{3}}, \\ \omega_1 &= -0.5 + \frac{\sqrt{3}}{2}i, \quad \omega_2 = -0.5 - \frac{\sqrt{3}}{2}i. \end{aligned} \quad (27)$$

Three possible solutions of the real root, z , exist depending upon the signs of Δ^* in Equation (27), as indicated in the following:

When $\Delta^* > 0$, the real root is

$$z_1 = F_1 + F_2 - \frac{E_1}{6}. \quad (28)$$

If $\Delta^* = 0$, then the real root becomes

$$z_1 = -\sqrt[3]{4q} - \frac{E_1}{6}. \quad (29)$$

However, if $\Delta^* < 0$, the real root is recovered in trigonometric form as

$$z_1 = 2\sqrt[3]{r} \cos\left(\frac{\alpha}{3}\right) - \frac{E_1}{6} \quad (30)$$

where

$$r = \sqrt{-\left(\frac{p}{3}\right)^3},$$

$$\alpha = \arccos\left(-\frac{q}{2r}\right). \quad (31)$$

Once the real root, z , is determined for Equation (21), the four roots of Equations (18) and (19) can then be expressed as

$$\Delta_2 = \frac{\xi_1^2}{4} - \phi_1, \quad \Delta_3 = \frac{\xi_2^2}{4} - \phi_2,$$

$$\psi_1 = -\frac{\xi_1}{2} + \sqrt{\Delta_2}, \quad \psi_2 = -\frac{\xi_1}{2} - \sqrt{\Delta_2},$$

$$\psi_3 = -\frac{\xi_2}{2} + \sqrt{\Delta_3}, \quad \psi_4 = -\frac{\xi_2}{2} - \sqrt{\Delta_3}. \quad (32)$$

The solutions are further complicated as a result of uncertainty in the signs of Δ_1 , Δ_2 , and Δ_3 . For a choice of representative physical parameters, Δ_1 is predominantly positive. The solutions due merely to the changing signs of Δ_2 and Δ_3 are reported in the following. For completeness, the solution for the negative Δ_1 is described in the Appendix.

2.1. SOLUTIONS WHEN $\Delta_1 \geq 0$, $\Delta_2 \geq 0$ AND $\Delta_3 \geq 0$

Concentration in the micropores may be determined from Equation (16) as

$$\bar{c}_2 = g_1 e^{\psi_1 y} + g_2 e^{\psi_2 y} + g_3 e^{\psi_3 y} + g_4 e^{\psi_4 y}, \quad (33)$$

where constants g_1, g_2, g_3 and g_4 are determined by satisfying the boundary conditions. The concentration in the macropores can be derived from Equation (15) as

$$\bar{c}_1 = \frac{1}{a\gamma}(\eta_1 g_1 e^{\psi_1 y} + \eta_2 g_2 e^{\psi_2 y} + \eta_3 g_3 e^{\psi_3 y} + \eta_4 g_4 e^{\psi_4 y}), \quad (34)$$

where

$$\begin{aligned} \eta_1 &= -\psi_1^2 + \frac{\gamma\psi_1}{b} - \gamma\beta_1, & \eta_2 &= -\psi_2^2 + \frac{\gamma\psi_2}{b} - \gamma\beta_1, \\ \eta_3 &= -\psi_3^2 + \frac{\gamma\psi_3}{b} - \gamma\beta_1, & \eta_4 &= -\psi_4^2 + \frac{\gamma\psi_4}{b} - \gamma\beta_1. \end{aligned} \quad (35)$$

A system of equations can be constructed through satisfying the boundary conditions given in Equation (10). After solving the system of equations through the method of elimination, the constants g_1, g_2, g_3 and g_4 are expressed as

$$g_1 = \frac{H_1}{M}, \quad g_2 = \frac{H_2}{M}, \quad g_3 = \frac{H_3}{M}, \quad g_4 = \frac{H^4}{M}, \quad (36)$$

and assume:

$$\begin{aligned} \eta_5 &= \psi_1 e^{\psi_1}, & \eta_6 &= \psi_2 e^{\psi_2}, & \eta_7 &= \psi_3 e^{\psi_3}, & \eta_8 &= \psi_4 e^{\psi_4}, \\ \eta_9 &= \eta_1 \eta_5, & \eta_{10} &= \eta_2 \eta_6, & \eta_{11} &= \eta_3 \eta_7, & \eta_{12} &= \eta_4 \eta_8 \\ \zeta_1 &= \frac{\bar{c}_1^0 a \gamma}{s}, & \zeta_2 &= \frac{\bar{c}_2^0}{s}, \end{aligned} \quad (37)$$

where

$$\begin{aligned} M &= (\eta_2 - \eta_1)(\eta_7 \eta_{12} - \eta_8 \eta_{11}) + (\eta_1 - \eta_3)(\eta_6 \eta_{12} - \eta_8 \eta_{10}) \\ &\quad + (\eta_4 - \eta_1)(\eta_6 \eta_{11} - \eta_7 \eta_{10}) + (\eta_3 - \eta_2)(\eta_5 \eta_{12} - \eta_8 \eta_9) \\ &\quad + (\eta_2 - \eta_4)(\eta_5 \eta_{11} - \eta_7 \eta_9) + (\eta_4 - \eta_3)(\eta_5 \eta_{10} - \eta_6 \eta_9). \end{aligned} \quad (38)$$

$$\begin{aligned} H_1 &= (\zeta_2 \eta_2 - \zeta_1)(\eta_7 \eta_{12} - \eta_8 \eta_{11}) + (\zeta_1 - \zeta_2 \eta_3)(\eta_6 \eta_{12} - \eta_8 \eta_{10}) \\ &\quad + (\zeta_2 \eta_4 - \zeta_1)(\eta_6 \eta_{11} - \eta_7 \eta_{10}) \end{aligned} \quad (39)$$

$$\begin{aligned} H_2 &= (\zeta_1 - \zeta_2 \eta_1)(\eta_7 \eta_{12} - \eta_8 \eta_{11}) + (\zeta_2 \eta_3 - \zeta_1)(\eta_5 \eta_{12} - \eta_8 \eta_9) \\ &\quad + (\zeta_1 - \zeta_2 \eta_4)(\eta_5 \eta_{11} - \eta_7 \eta_9). \end{aligned} \quad (40)$$

$$H_3 = (\zeta_2 \eta_1 - \zeta_1)(\eta_6 \eta_{12} - \eta_8 \eta_{10}) + (\zeta_1 - \zeta_2 \eta_3)(\eta_5 \eta_{12} - \eta_8 \eta_9)$$

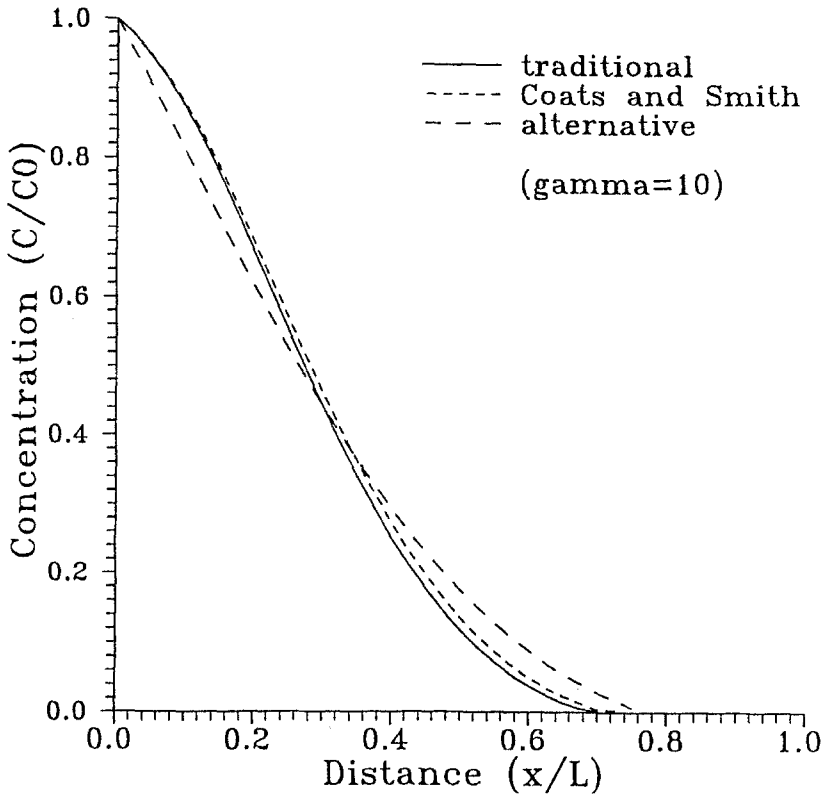


Fig. 2. Comparison of spatial concentration when $\gamma = 10$.

$$+ (\zeta_2 \eta_4 - \zeta_1)(\eta_5 \eta_{10} - \eta_6 \eta_9) \quad (41)$$

$$\begin{aligned}
 H_4 = & (\zeta_1 - \zeta_2 \eta_1)(\eta_6 \eta_{11} - \eta_7 \eta_{10}) + (\zeta_2 \eta_2 - \zeta_1)(\eta_5 \eta_{11} - \eta_7 \eta_9) \\
 & + (\zeta_1 - \zeta_2 \eta_3)(\eta_5 \eta_{10} - \eta_6 \eta_9). \quad (42)
 \end{aligned}$$

2.2. SOLUTIONS WHEN $\Delta_1 \geq 0, \Delta_2 < 0$ AND $\Delta_3 \geq 0$

For this condition, two of the four roots from Equations (18) and (19) become complex variables, and may be rewritten as

$$\psi_1 = -\frac{\xi_1}{2} + i\sqrt{-\Delta_2}, \quad \psi_2 = -\frac{\xi_1}{2} - i\sqrt{-\Delta_2}. \quad (43)$$

ψ_3 and ψ_4 are unchanged from Equation (32). The concentration in micropores can be alternatively expressed as

$$\bar{c}_2 = g_1 e^{w_1 y} \cos(w_2 y) + g_2 e^{w_1 y} \sin(w_2 y) + g_3 e^{\psi_3 y} + g_4 e^{\psi_4 y}, \quad (44)$$

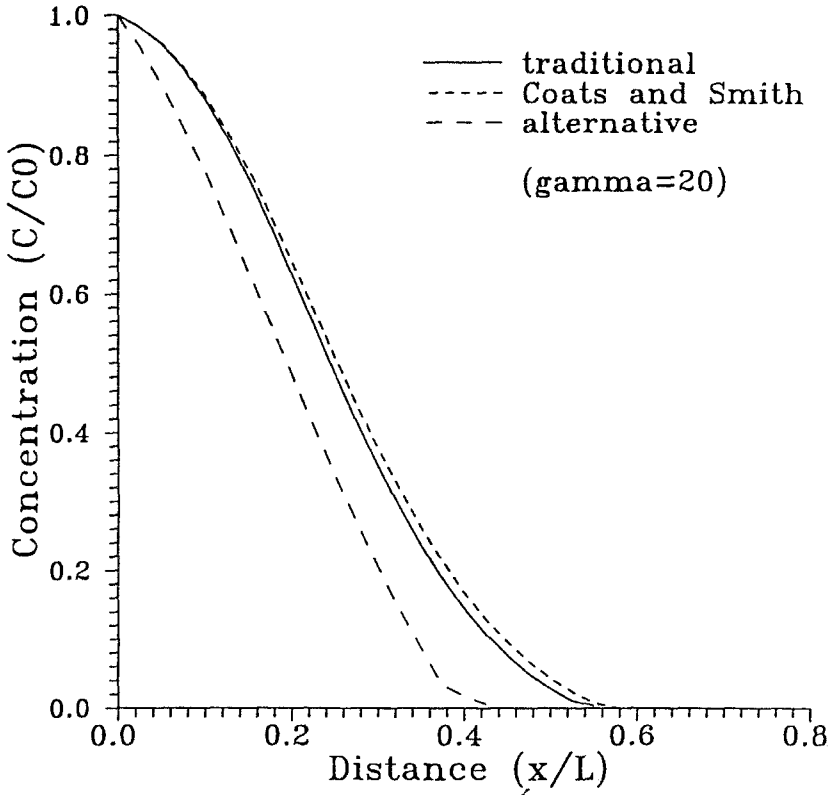


Fig. 3. Comparison of spatial concentration when $\gamma = 20$.

where

$$w_1 = -\frac{\xi_1}{2}, \quad w_2 = \sqrt{-\Delta_2}. \quad (45)$$

Similarly, the concentration within the macropores is described as

$$\begin{aligned} \bar{c}_1 = \frac{1}{a\gamma} \{ & g_1 e^{w_1 y} [\lambda_1 \cos(w_2 y) - \lambda_2 \sin(w_2 y)] \\ & + g_2 e^{w_1 y} [\lambda_1 \sin(w_2 y) + \lambda_2 \cos(w_2 y)] \\ & + \lambda_3 g_3 e^{\psi_3 y} + \lambda_4 g_4 e^{\psi_4 y} \}, \end{aligned} \quad (46)$$

where

$$\begin{aligned} \lambda_1 = -w_1^2 + w_2^2 + w_1 \frac{\gamma}{b} - \gamma\beta_1, \quad \lambda_2 = -w_2 \left(2w_1 - \frac{\gamma}{b} \right), \\ \lambda_3 = -\psi_3^2 + \frac{\gamma\psi_3}{b} - \gamma\beta_1, \quad \lambda_4 = -\psi_4^2 + \frac{\gamma\psi_4}{b} - \gamma\beta_1. \end{aligned} \quad (47)$$

For convenience, assume

$$\begin{aligned}
 \alpha_1 &= e^{w_1}[w_1 \cos(w_2) - w_2 \sin(w_2)], \\
 \alpha_2 &= e^{w_1}[w_1 \sin(w_2) + w_2 \cos(w_2)], \\
 \alpha_3 &= \psi_3 e^{\psi_3}, \quad \alpha_4 = \psi_4 e^{\psi_4}, \\
 \alpha_5 &= e^{w_1}[(\lambda_1 w_1 - \lambda_2 w_2) \cos(w_2) - (\lambda_2 w_1 + \lambda_1 w_2) \sin(w_2)], \\
 \alpha_6 &= e^{w_1}[(\lambda_1 w_2 + \lambda_2 w_1) \cos(w_2) + (\lambda_2 w_1 - \lambda_1 w_2) \sin(w_2)], \\
 \alpha_7 &= \lambda_3 \alpha_3, \quad \alpha_8 = \lambda_4 \alpha_4.
 \end{aligned} \tag{48}$$

Following a similar procedure as previously, the constants g_1, g_2, g_3 and g_4 in Equations (44) and (46) are derived as in Equation (36) but with the substitution of M and $H_i (i = 1, 2, 3, 4)$ as

$$\begin{aligned}
 M &= (\alpha_2 \alpha_7 - \alpha_3 \alpha_6)(\lambda_1 + \lambda_4) + (\alpha_2 \alpha_8 - \alpha_4 \alpha_6) \\
 &\quad (\lambda_1 - \lambda_3) + (\alpha_1 \alpha_6 - \alpha_2 \alpha_5)(\lambda_4 - \lambda_3) \\
 &\quad + \lambda_2 [\alpha_8(\alpha_3 - \alpha_1) + \alpha_4(\alpha_5 - \alpha_7) + \alpha_1 \alpha_7 - \alpha_3 \alpha_5].
 \end{aligned} \tag{49}$$

$$\begin{aligned}
 H_1 &= \zeta_2 [\lambda_2 (\alpha_3 \alpha_8 - \alpha_4 \alpha_7) - \lambda_3 (\alpha_2 \alpha_8 - \alpha_4 \alpha_6) + \lambda_4 (\alpha_2 \alpha_7 - \alpha_3 \alpha_6)] \\
 &\quad - \zeta_1 (\alpha_4 \alpha_6 - \alpha_2 \alpha_8 + \alpha_2 \alpha_7 - \alpha_3 \alpha_6).
 \end{aligned} \tag{50}$$

$$\begin{aligned}
 H_2 &= -\zeta_2 [\lambda_1 (\alpha_3 \alpha_8 - \alpha_4 \alpha_7) - \lambda_3 (\alpha_1 \alpha_8 - \alpha_4 \alpha_5) + \lambda_4 (\alpha_1 \alpha_7 - \alpha_3 \alpha_5)] \\
 &\quad + \zeta_1 (\alpha_3 \alpha_8 - \alpha_4 \alpha_7 - \alpha_1 \alpha_8 + \alpha_4 \alpha_5 + \alpha_1 \alpha_7 - \alpha_3 \alpha_5).
 \end{aligned} \tag{51}$$

$$\begin{aligned}
 H_3 &= \zeta_2 [\lambda_1 (\alpha_2 \alpha_8 - \alpha_4 \alpha_6) - \lambda_2 (\alpha_1 \alpha_8 - \alpha_4 \alpha_5) + \lambda_4 (\alpha_1 \alpha_6 - \alpha_2 \alpha_5)] \\
 &\quad - \zeta_1 (\alpha_2 \alpha_8 - \alpha_4 \alpha_6 + \alpha_1 \alpha_6 - \alpha_2 \alpha_5).
 \end{aligned} \tag{52}$$

$$\begin{aligned}
 H_4 &= -\zeta_2 [\lambda_1 (\alpha_2 \alpha_7 - \alpha_3 \alpha_6) - \lambda_2 (\alpha_1 \alpha_7 - \alpha_3 \alpha_5) + \lambda_3 (\alpha_1 \alpha_6 - \alpha_2 \alpha_5)] \\
 &\quad + \zeta_1 (\alpha_2 \alpha_7 - \alpha_3 \alpha_6 + \alpha_1 \alpha_6 - \alpha_2 \alpha_5).
 \end{aligned} \tag{53}$$

2.3. SOLUTIONS WHEN $\Delta_1 \geq 0, \Delta_2 < 0$ AND $\Delta_3 < 0$

Under this condition, all four roots from Equations (18) and (19) become complex variables. ψ_1 and ψ_2 have identical forms to equation (43). ψ_3 and ψ_4 are

$$\psi_3 = -\frac{\xi_2}{2} + i\sqrt{-\Delta_3}, \quad \psi_4 = -\frac{\xi_2}{2} - i\sqrt{-\Delta_3}. \tag{54}$$

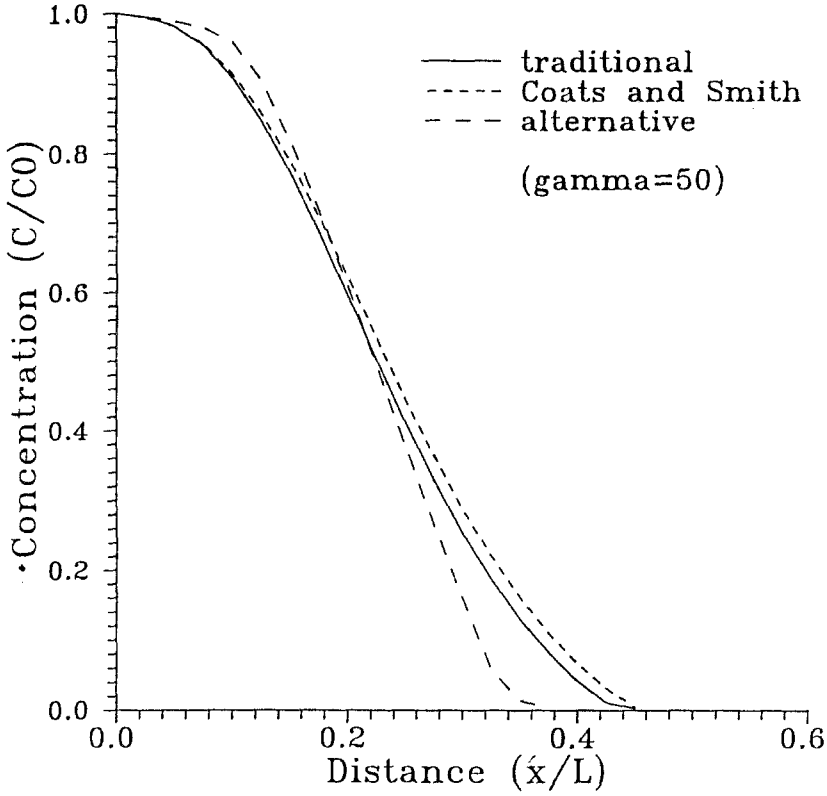


Fig. 4. Comparison of spatial concentration when $\gamma = 50$.

The concentration in micropores can be written as

$$\begin{aligned} \bar{c}_2 = & g_1 e^{w_1^* y} \cos(w_2^* y) + g_2 e^{w_1^* y} \sin(w_2^* y) \\ & + g_3 e^{w_3^* y} \cos(w_4^* y) + g_4 e^{w_3^* y} \sin(w_4^* y), \end{aligned} \quad (55)$$

where w_1^* and w_2^* are identical to w_1 and w_2 given in Equation (45), with w_3^* and w_4^* defined as

$$w_3^* = -\frac{\xi_2}{2}, \quad w_4^* = \sqrt{-\Delta_3}. \quad (56)$$

The concentration in macropores can be derived as

$$\begin{aligned} \bar{c}_1 = & \frac{1}{a\gamma} \{ g_1 e^{w_1^* y} [\lambda_1 \cos(w_2^* y) - \lambda_3 \sin(w_2^* y)] \\ & + g_2 e^{w_1^* y} [\lambda_1 \sin(w_2^* y) + \lambda_3 \cos(w_2^* y)] \} \end{aligned}$$

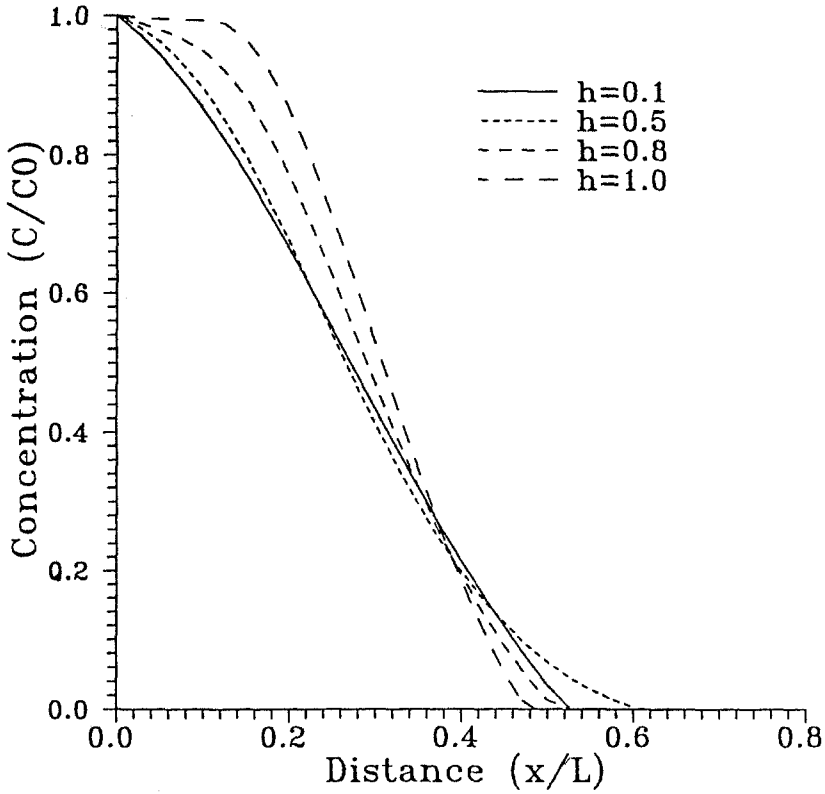


Fig. 5. Spatial concentration for various 'h'.

$$\begin{aligned}
 &+ g_3 e^{w_3^* y} [\lambda_2 \cos(w_4^* y) - \lambda_4 \sin(w_4^* y)] \\
 &+ g_4 e^{w_3^* y} [\lambda_2 \sin(w_4^* y) + \lambda_4 \cos(w_4^* y)] \}, \quad (57)
 \end{aligned}$$

where

$$\begin{aligned}
 \lambda_1 &= -(w_1^*)^2 + (w_2^*)^2 + w_1^* \frac{\gamma}{b} - \gamma \beta_1, \\
 \lambda_2 &= -(w_3^*)^2 + (w_4^*)^2 + w_3^* \frac{\gamma}{b} - \gamma \beta_1, \\
 \lambda_3 &= -w_2^* \left(2w_1^* - \frac{\gamma}{b} \right), \quad \lambda_4 = -w_4^* \left(2w_3^* - \frac{\gamma}{b} \right). \quad (58)
 \end{aligned}$$

After satisfying the boundary conditions, the system of equations for obtaining the constants $g_1, g_2, g_3,$ and g_4 can be constructed as follows:

$$\begin{bmatrix} 1 & 0 & 1 & 0 \\ \lambda_1 & \lambda_3 & \lambda_2 & \lambda_4 \\ \alpha_1 & \alpha_2 & \alpha_3 & \alpha_4 \\ \alpha_5 & \alpha_6 & \alpha_7 & \alpha_8 \end{bmatrix} \begin{bmatrix} g_1 \\ g_2 \\ g_3 \\ g_4 \end{bmatrix} = \begin{bmatrix} \zeta_2 \\ \zeta_1 \\ 0 \\ 0 \end{bmatrix} \quad (59)$$

where

$$\begin{aligned} \alpha_1 &= e^{w_1^*} [w_1^* \cos(w_2^*) - w_2^* \sin(w_2^*)], \\ \alpha_2 &= e^{w_1^*} [w_1^* \sin(w_2^*) + w_2^* \cos(w_2^*)], \\ \alpha_3 &= e^{w_3^*} [w_3^* \cos(w_4^*) - w_4^* \sin(w_4^*)], \\ \alpha_4 &= e^{w_3^*} [w_3^* \sin(w_4^*) + w_4^* \cos(w_4^*)], \\ \alpha_5 &= e^{w_1^*} [(\lambda_1 w_1^* - \lambda_3 w_2^*) \cos(w_2^*) - (\lambda_3 w_1^* + \lambda_1 w_2^*) \sin(w_2^*)], \\ \alpha_6 &= e^{w_1^*} [(\lambda_1 w_2^* + \lambda_3 w_1^*) \cos(w_2^*) + (\lambda_1 w_1^* - \lambda_3 w_2^*) \sin(w_2^*)], \\ \alpha_7 &= e^{w_3^*} [(\lambda_2 w_3^* - \lambda_4 w_4^*) \cos(w_4^*) - (\lambda_4 w_3^* + \lambda_2 w_4^*) \sin(w_4^*)], \\ \alpha_8 &= e^{w_3^*} [(\lambda_4 w_3^* + \lambda_2 w_4^*) \cos(w_4^*) + (\lambda_2 w_3^* + \lambda_4 w_4^*) \sin(w_4^*)]. \end{aligned} \quad (60)$$

Because the condition of $\Delta_3 < 0$ is unlikely encountered for parameters selected in the present study, detailed discussion of the solution of Equation (59) is omitted.

Solute concentrations c_1 and c_2 may be recovered in time by invoking a numerical inversion technique. In this work the Stehfest algorithm (Stehfest, 1970) is utilized.

3. Modeling of Miscible Flow

The model incorporating micropore diffusion and convection developed in this paper is compared to the analytical results obtained from a conventional dispersion-convection model (Bear, 1972), and to the model developed by Coats and Smith (1964). The sensitivity of the model is tested through parametric investigation. The model is also verified against experimental data. The relative concentration is represented for the macropore space only. Table I summarizes the selected modeling parameters for the designated figures.

The comparison of spatial concentration between the conventional single-porosity model (SP), the Coats and Smith's model (CS) and the present model (DP) for various equivalent Péclet numbers, γ , is shown in Figures 2–4. For the

TABLE I. Parameters for analytical modeling

Fig.	γ	f	a	h	b	c_1^0	c_2^0	τ	y
2	10	0.95	0.1	0.4	1.25	1	0.8	0.2	0-1
3	20	0.95	0.1	0.4	1.25	1	0.8	0.2	0-1
4	50	0.95	0.1	0.4	1.25	1	0.8	0.2	0-1
5	50	0.9	0.1	0.1-1	2	1	0.5	0.2	0-1
6	50	0.5-0.9	0.1	0.5	2	1	0.5	0.2	0-1
7	50	0.9	0.1-10	0.5	2	1	0.5	0.2	0-1
8	50	0.9	0.1	0.5	1-10	1	0.2	0.2	0-1
9	50	0.9	0.1	0.5	2	1	0.1-0.9	0.2	0-1
10	50	0.9	0.1	0.5	2	1	0.5	0-2	0.1-0.9
11	50	0.9	0.1	0.01-0.5	2	1	0.5	0-2	0.5
12	1-100	0.9	0.1	0.5	2	1	0.5	0-1	0.5
13	50	0.9	0.1	0.5	2-50	1	0.5	0-1	0.5
14	80	0.9	0.1	0.4	1.25	1	0.9	0.4-1.2	0.9

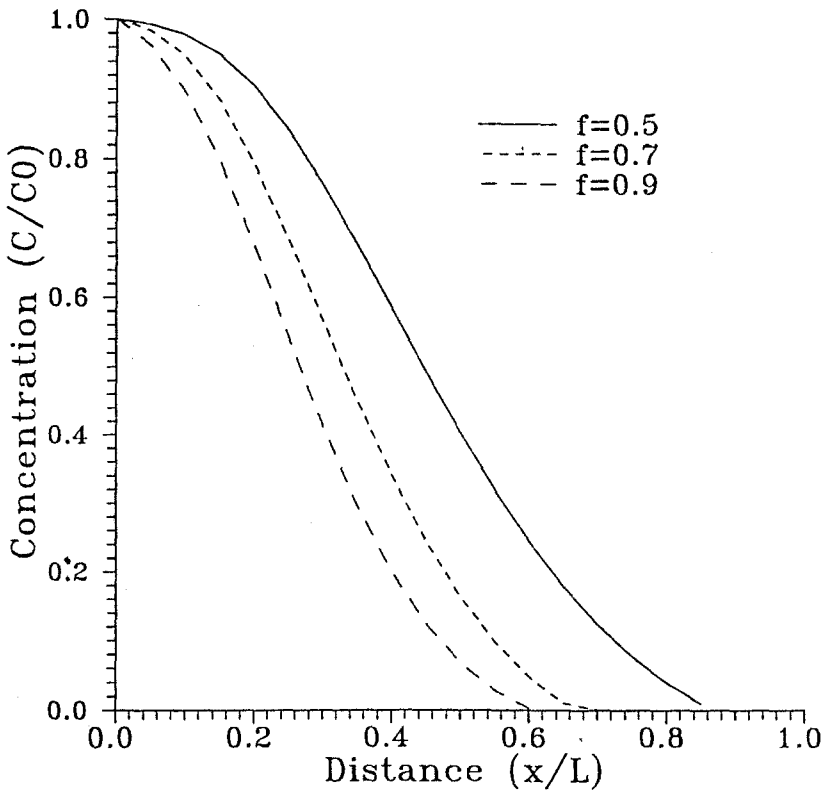


Fig. 6. Spatial concentration for various 'f'.

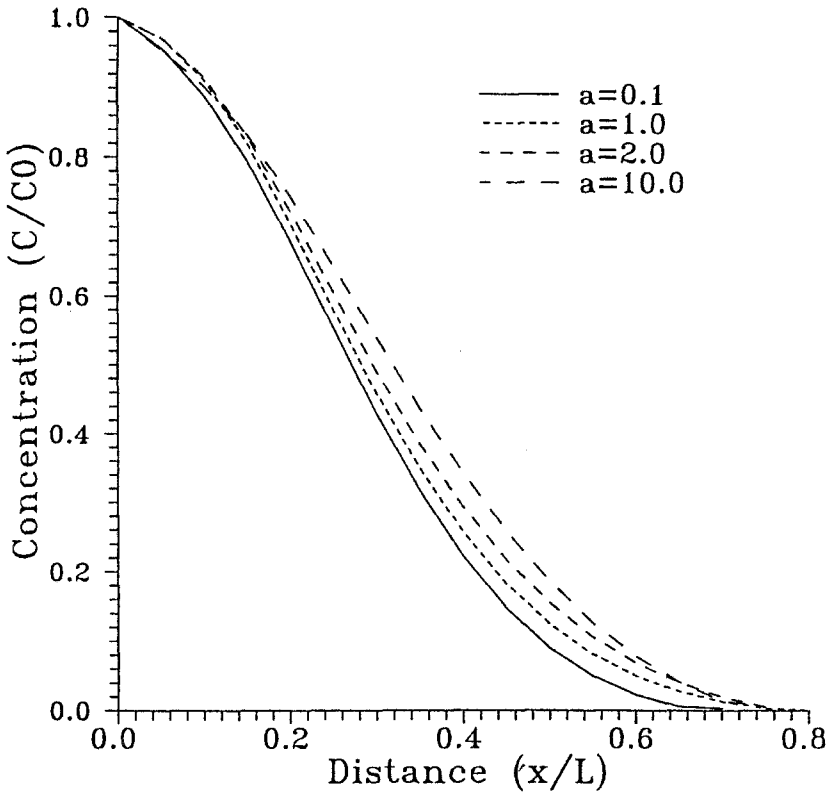


Fig. 7. Spatial concentration for various 'a'.

dispersion dominated case, Figure 2 indicates a good match between the SP and CS models, whereas the result from the DP model appears to be comparatively more diffusive at both upstream and downstream locations. The flow in micropores contributes very little to the concentration change in the central portion of the solute transport front with insignificant local flow velocity. The disparity between the present model and the other two models becomes more apparent as γ increases (Figure 3), due to the dominance of the flow in macropores. The most significant difference occurs in locations remote from the source. In view of the difference between the CS and DP models, the apparent time lag is attributed to the dominant diffusion and less dominant convection within the micropores. The spatial concentration profile can be dramatically modified as γ increases further (Figure 4). In comparison, convection becomes more pervasive than diffusion within the micropores, resulting in a sharper moving front for the DP model. It is of interest to note that, although the CS model is also based on a multi-component mechanism, no significant difference can be readily identified between the CS model and traditional SP model for the present analysis. Therefore, modeling the mechanism

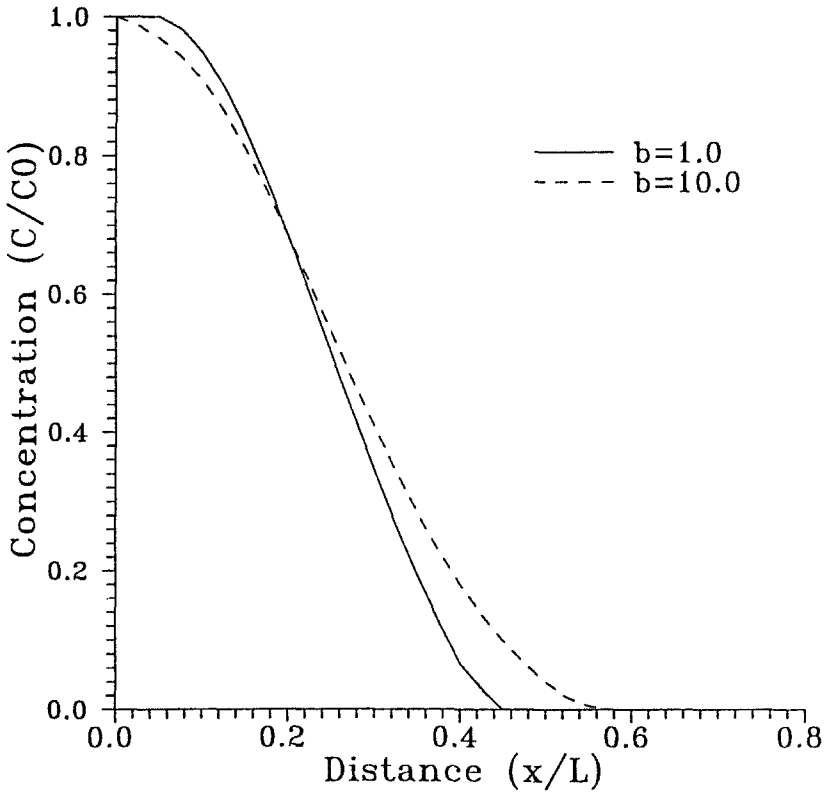


Fig. 8. Spatial concentration for various ' b '.

of transport within micropores indeed provides additional flexibilities to matching the experimental data.

The equivalent Peclet number γ indexes the ratio between macropore convection and micropore dispersion. As shown in Figure 2–4, the values of γ control the profiles of solute concentration, with larger γ representing sharper front. The solute concentration profiles are also regulated by the ratio of dispersion (h) between micropores and macropores. Accurate definition of hydrodynamic dispersion should include both molecular diffusion due to concentration gradient and mechanical dispersion as a result of velocity variations. In multi-component media, diffusion is likely to dominate behavior in micropores of low velocity regions, in contrast to the dispersion dominated macropore areas where flow rate is relatively more substantial. For completeness, however, this difference is not emphasized in this study. In general, h is less than unity (Sardin and Schweich, 1991). As depicted by Figure 5, smaller h , reflecting more significant dispersion in macropores, results in the dominant diffusive type of transport. As h increases, the macro dispersion is progressively overshadowed by the dispersive flow within micropores; consequently, convective flow becomes more influential in the transport process. On the

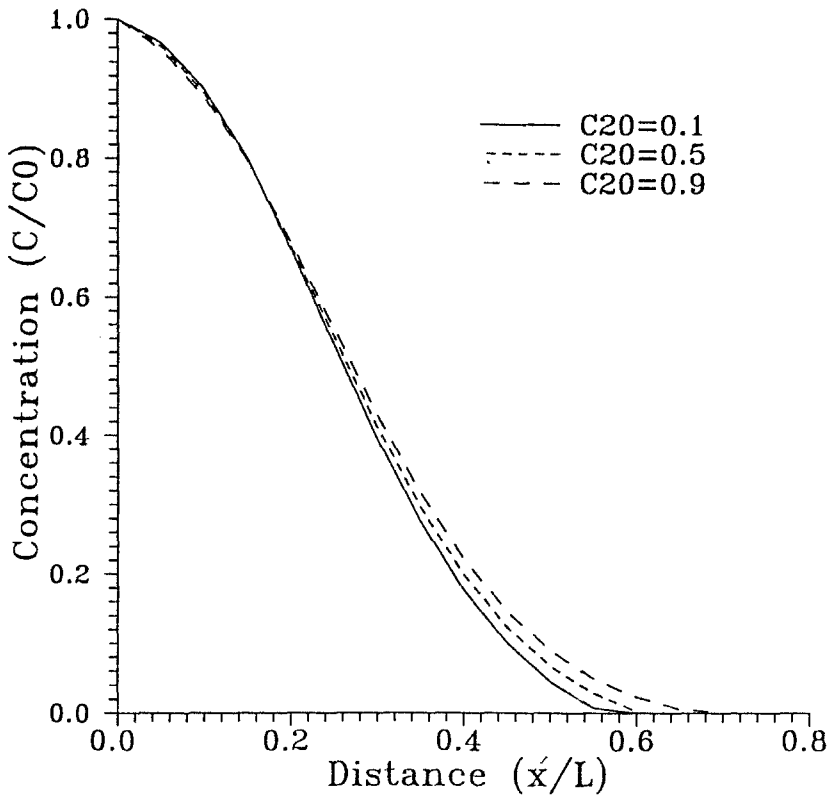


Fig. 9. Spatial concentration for various ' c_2^0 '.

other hand, larger h represents more prominent macropore-micropore interaction, which leads to more localized concentration changes.

The factor f represents the percentage of pore space taken by the fluid traveling through macropores. For transport under the condition that $f \rightarrow 1$, the response resembles the normal dispersion-convection process. Reduced f reflects the more obvious effect of the transport in micropores, which leads to the activities of more localized solute attenuation. This effect appears to be significant and is depicted in Figure 6.

The magnitude of the coefficient a describes the intensity of the interporosity flow between macropores and micropores. As depicted in Figure 7, larger a corresponds to a greater exchange rate, and results in more linear and extensive solute spreading away from the source area. For smaller a , the effect of variation in the interporosity rate appears to be less significant.

The coefficient b defines the proportionality of flow velocity between macropores and micropores and is typically greater than unity (Gerke and Van Genuchten, 1993). For comparison purpose, Figures 8 illustrates the spatial concentration changes for various magnitudes of the coefficient b . The smoothed, typically dif-

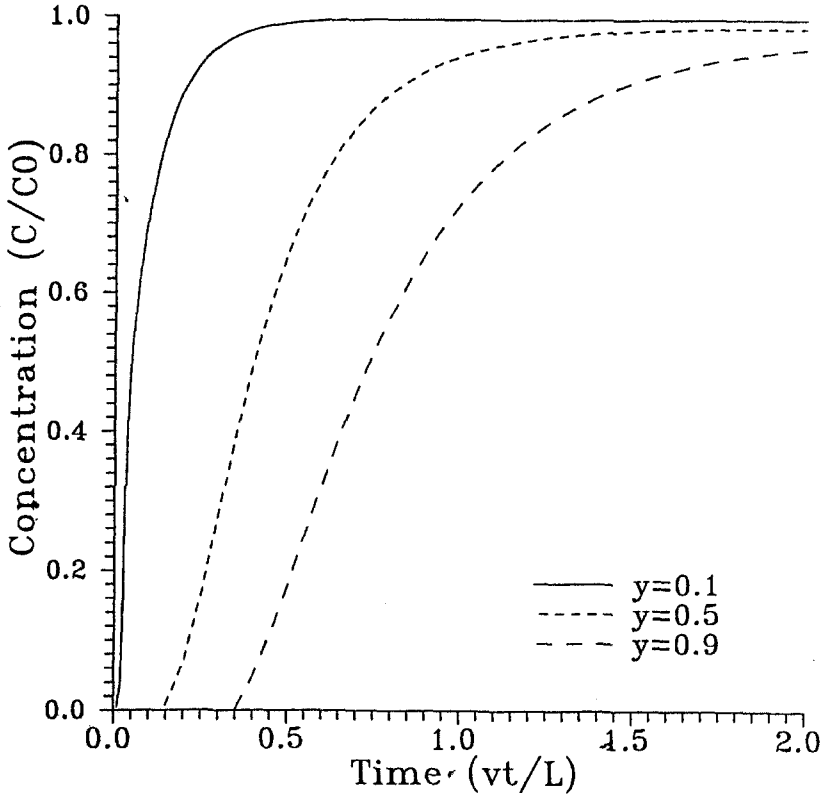


Fig. 10. Breakthrough curves for various 'y'.

fusive concentration curve is generated for the case with larger b , which reflects the reduced interactive flow between macropores and micropores, or dominant flow within macropores. In contrast, the sharper solute front appears to be associated with the case using smaller b , which is likely attributed to the increasing modification on solute concentration due to prominent flow within micropores.

The concentration gradient between macropores and micropores at the source location may provide a noticeable effect on the degree of mass interaction between the two media. As shown in Figure 9, smaller c_2^0 represents larger concentration difference, consequently results in the more dramatic interporosity transport, and thus more localized change of concentration. Conversely, larger c_2^0 corresponds to reduced constraint to the flow in macropores due to micropore flow, and therefore promotes more extensive solute migration. However, the effect of change in c_2^0 appears to be less significant.

The temporal variation of concentration at various positions relative to the source location is illustrated in Figure 10. Solute breakthrough is more abrupt at the locations near the source since the dispersive behavior is less fully developed. The tailing of the response is more apparent at the places remote from the source. Since

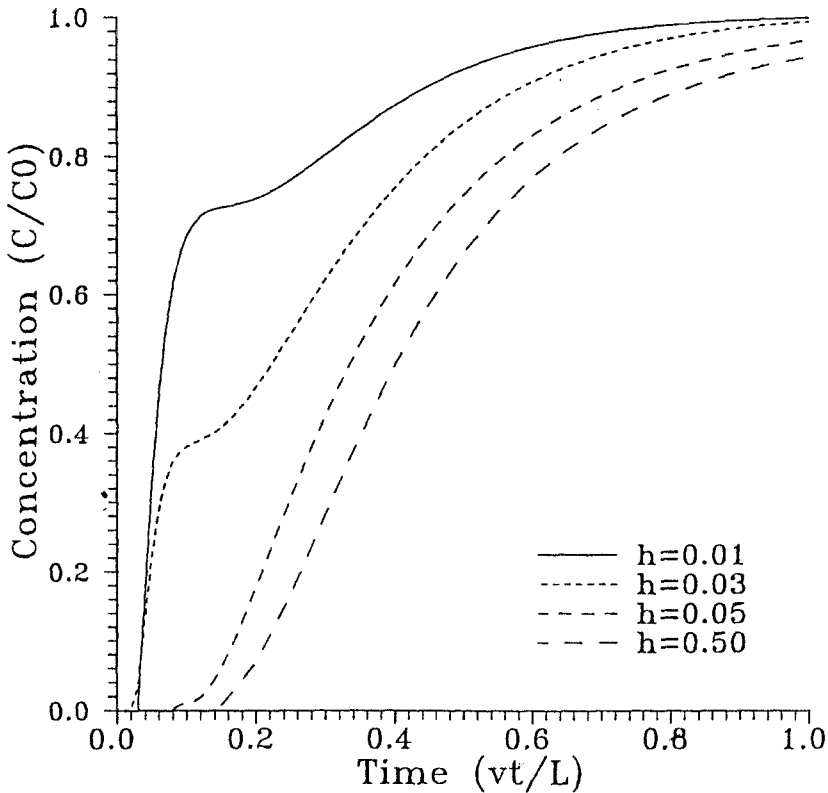


Fig. 11. Breakthrough curves for various 'h'.

the tailing is usually considered to be the result of capacitance effects, the impact of micropore flow becomes more significant at lower local flow velocities.

For various values of h , different breakthrough curves are described in Figure 11. It is particularly interesting to note that the slope changes of the relative concentration occur for smaller h . This phenomenon, indicating the interporosity solute exchange between macropores and micropores, cannot be revealed by a conventional dispersion-convection model. This variable change of solute concentration in breakthrough profiles has been reported in the laboratory for single fracture column tests (Neretnieks, 1993). As mentioned previously, smaller h represents the dominant dispersion in macropores. Under this scenario, the solute breakthrough at the examined point can be so rapid and abrupt that the miscible displacement may be temporarily slowed down due to the decrease of mass in macropores until receiving sufficient mass replenishment from micropores. For larger h , the development of dispersion in macropores and micropores is harmonic. As a result, the breakthrough curve follows a similar trend as in a homogeneous medium, except that the extended tailing in the curve may appear due to the influence of micropore transport.

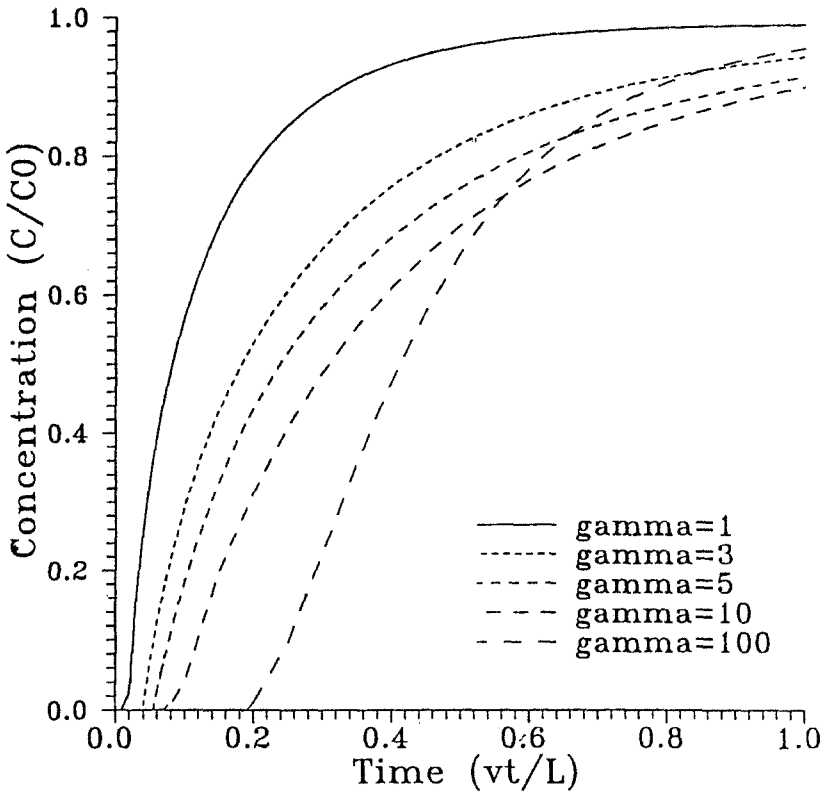


Fig. 12. Breakthrough curves for various ' γ '.

The equivalent Peclet number γ exerts significant influence on the temporal change of solute, as shown in Figure 12. For the cases with smaller γ , breakthrough profiles appear to possess the patterns of sudden occurrence accompanied by the extensive tailing. For the significantly larger γ , the breakthrough curve appears to follow a regular style, depicting a pronounced mechanical dispersion process in macropores.

The influence of velocity ratio b on the breakthrough curves is illustrated in Figure 13. It is seen that the excessive tailing may be attributed to the increase of the velocity contrast between macropores and micropores. The variation of b , however, appears to have little impact on the initial occurrence of solute.

Bouhroum (1993) presented the results from miscible displacement experiments which were performed on two parallelepipedal prototypes with NaCl–water solution (0.25 g/l). The prototypes were made of plexiglas to observe the migration of dye tracer injected simultaneously with NaCl. The in situ conductivity measurement techniques equipped with conductivity detectors were utilized to provide time variation of concentration at different distance from the inlet. Selecting identical dimensionless time and location and adjusting other parameters shown in Table I,

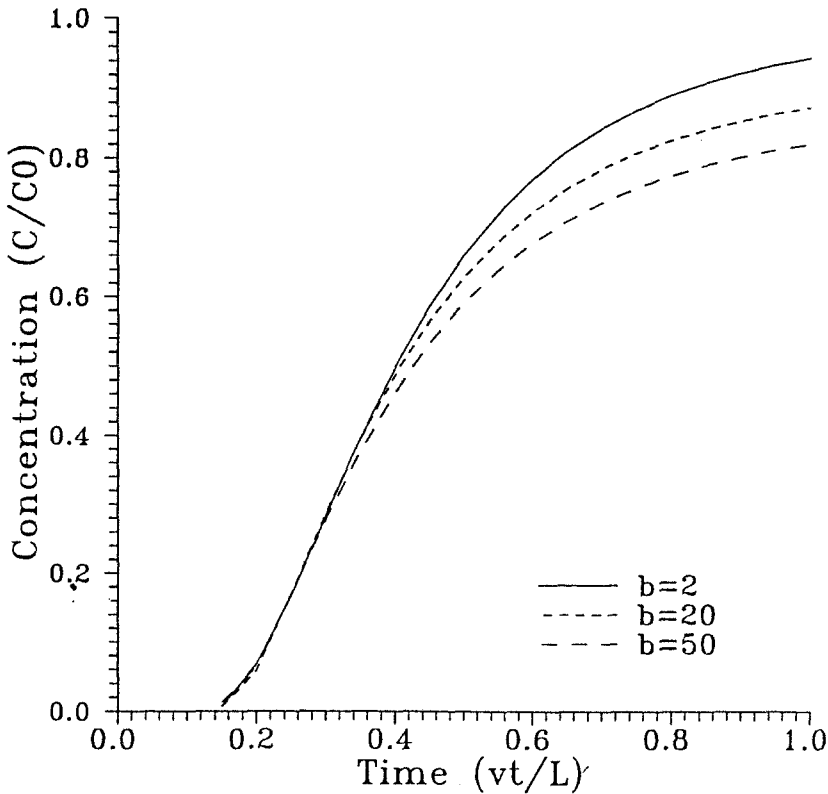


Fig. 13. Breakthrough curves for various 'b'.

the result of using the present model has been compared with the experimental data reported by Bouhroum (1993), as depicted in Figure 14. A match with good accuracy between the modeling result and the test data is readily recognized. Although it may not reflect the true physical mechanism of solute transport through heterogeneous porous media, the excellent agreement indeed demonstrates the added flexibilities of using the proposed model.

4. Conclusions

A model is presented to represent miscible flow in strongly heterogeneous media. This model utilizes the concept of micropore convection and diffusion as an alternative to the assumption of stagnant liquid in micropores, as postulated in current capacitance models. This alternative conceptualization is shown to represent the heterogeneity of porous media on a more realistic and complete physical basis. Unusual transport behavior, including abrupt early solute breakthrough and lengthly tailing that are frequently observed is readily accommodated by allowing the local diffusive and convective flow to develop, and proceed, within micropore space. This local effect is also shown to result in a rapidly moving, but more dif-

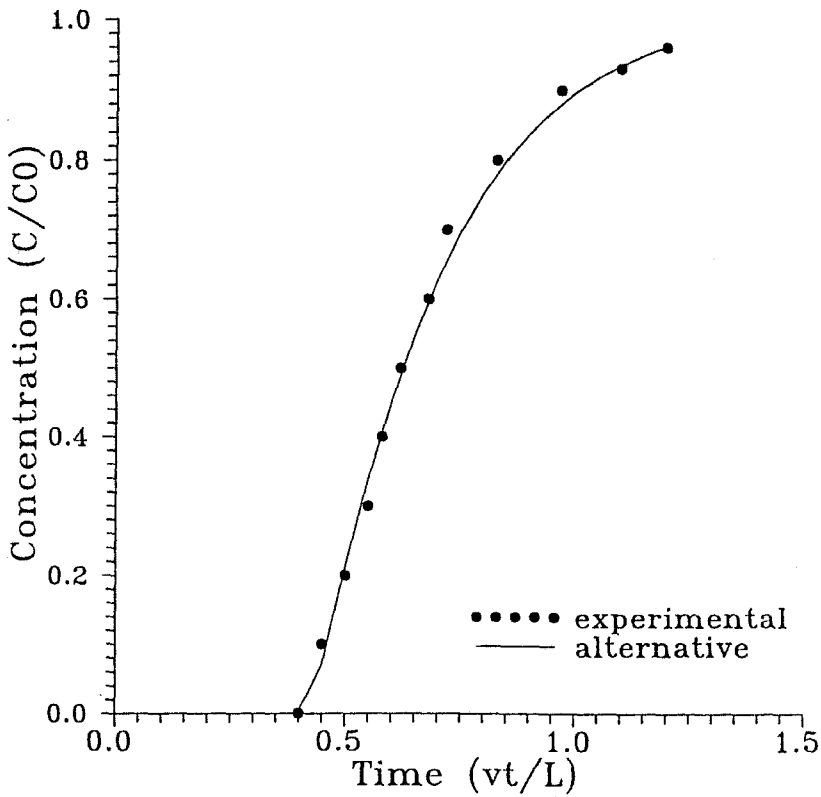


Fig. 14. Comparison of breakthrough curves

fusive, migration front. Comparative study reveals apparent flexibilities added to the present model, beneficial to matching with laboratory and field measurements. Variable concentration changes are identified in the analysis of solute breakthrough, analogous to the dual-porosity behavior of fractured porous media. The mathematical formulation of this new conceptualization leads to a coupled partial differential equation. Analytical solutions have been obtained by invoking the method of differential operators in Laplace domain. From a practical stand point, the additional attenuation mechanism present in representing the micropore diffusion and convection effects give added flexibility in replicating observed response in strongly heterogeneous media. The analytical solutions provide utilities in approximating the 'real' physical processes present in the system, depicted as solute attenuation as a result of diffusive and convective flow into and out of low-velocity pore spaces.

Appendix: Solutions when $\Delta_1 < 0$

If $\Delta_1 < 0$, then ξ_1, ξ_2, ϕ_1 and ϕ_2 in Equation (20) all become complex variables such as:

$$\begin{aligned}\xi_1 &= 0.5(B_1 + i\sqrt{-\Delta_1}), & \xi_2 &= 0.5(B_1 - i\sqrt{-\Delta_1}), \\ \phi_1 &= z - i\frac{B_1z - B_3}{\sqrt{-\Delta_1}}, & \phi_2 &= z + i\frac{B_1z - B_3}{\sqrt{-\Delta_1}}.\end{aligned}\quad (61)$$

The respective four roots of Equations (18) and (19) can be determined as

$$\psi_1 = W_1 + iW_2, \quad (62)$$

where

$$R_1 = \frac{1}{16}(B_1^2 + \Delta_1) - z,$$

$$R_2 = \frac{B_1\sqrt{-\Delta_1}}{8} + \frac{B_1z - B_3}{\sqrt{-\Delta_1}},$$

$$\alpha^* = 0.5 \arctan\left(\frac{R_2}{R_1}\right),$$

$$W_1 = -0.25B_1 + (R_1^2 + R_2^2)^{0.25} \cos(\alpha^*),$$

$$W_2 = (R_1^2 + R_2^2)^{0.25} \sin(\alpha^*) - 0.25\sqrt{-\Delta_1}. \quad (63)$$

$$\psi_2 = W_3 - iW_4, \quad (64)$$

where

$$W_3 = -0.25B_1 - (R_1^2 + R_2^2)^{0.25} \cos(\alpha^*),$$

$$W_4 = (R_1^2 + R_2^2)^{0.25} \sin(\alpha^*) + 0.25\sqrt{-\Delta_1}. \quad (65)$$

$$\psi_3 = W_1 - iW_2, \quad (66)$$

and

$$\psi_4 = W_3 + iW_4. \quad (67)$$

The form of the solution depends on the signs of W_2 and W_4 . If $W_2 \geq 0$ and $W_4 \geq 0$, then one has

$$\begin{aligned}\bar{c}_2 &= g_1 e^{W_1 y} \cos(W_2 y) + g_2 e^{W_3 y} \sin(W_4 y) \\ &+ g_3 e^{W_1 y} \sin(W_2 y) + g_4 e^{W_3 y} \cos(W_4 y),\end{aligned}\quad (68)$$

and

$$\begin{aligned}\bar{c}_1 = & \frac{1}{a\gamma} \{g_1 e^{W_1 y} [\lambda_1 \cos(W_2 y) - \lambda_2 \sin(W_2 y)] \\ & + g_2 e^{W_3 y} [\lambda_3 \cos(W_4 y) + \lambda_4 \sin(W_4 y)] \\ & + g_3 e^{W_1 y} [\lambda_2 \cos(W_2 y) + \lambda_1 \sin(W_2 y)] \\ & + g_4 e^{W_3 y} [\lambda_4 \cos(W_4 y) - \lambda_3 \sin(W_4 y)]\} \quad (69)\end{aligned}$$

where

$$\begin{aligned}\lambda_1 = & -W_1^2 + W_1^2 + W_1 \frac{\gamma}{b} - \gamma\beta_1, & \lambda_2 = & -W_2 \left(2W_1 - \frac{\gamma}{b}\right), \\ \lambda_3 = & -W_4 \left(2W_3 - \frac{\gamma}{b}\right), & \lambda_4 = & -W_3^2 + W_4^2 + W_3 \frac{\gamma}{b} - \gamma\beta_1.\end{aligned} \quad (70)$$

Assuming

$$\begin{aligned}\alpha_1 = & e^{W_1} [W_1 \cos(W_2) - W_2 \sin(W_2)], \\ \alpha_2 = & e^{W_3} [W_3 \sin(W_4) + W_4 \cos(W_4)], \\ \alpha_3 = & e^{W_1} [W_1 \sin(W_2) + W_2 \cos(W_2)], \\ \alpha_4 = & e^{W_3} [W_3 \cos(W_4) - W_4 \sin(W_4)], \\ \alpha_5 = & e^{W_1} [(\lambda_1 W_1 - \lambda_2 W_2) \cos(W_2) - (\lambda_2 W_1 + \lambda_1 W_2) \sin(W_2)], \\ \alpha_6 = & e^{W_3} [(\lambda_3 W_3 + \lambda_4 W_4) \cos(W_4) + (\lambda_4 W_3 - \lambda_3 W_4) \sin(W_4)], \\ \alpha_7 = & e^{W_1} [(\lambda_2 W_1 + \lambda_1 W_2) \cos(W_2) + (\lambda_1 W_1 - \lambda_2 W_2) \sin(W_2)], \\ \alpha_8 = & e^{W_3} [(\lambda_4 W_3 - \lambda_3 W_4) \cos(W_4) - (\lambda_3 W_3 + \lambda_4 W_4) \sin(W_4)]. \quad (71)\end{aligned}$$

After satisfying the boundary conditions, the constants g_1, g_2, g_3 and g_4 in Equations (68) and (69) are derived as follows:

$$g_1 = \frac{H_1^*}{M^*}, \quad g_2 = \frac{H_2^*}{M^*}, \quad g_3 = \frac{H_3^*}{M^*}, \quad g_4 = \frac{H_4^*}{M^*}, \quad (72)$$

where

$$\begin{aligned}M^* = & \lambda_2 [\alpha_3 (\alpha_8 - \alpha_5) + \alpha_7 (\alpha_1 - \alpha_4)] - \lambda_3 [\alpha_2 (\alpha_8 - \alpha_5) + \alpha_6 (\alpha_1 - \alpha_4)] \\ & + (\lambda_4 - \lambda_1) (\alpha_2 \alpha_7 - \alpha_3 \alpha_6).\end{aligned} \quad (73)$$

$$H_1^* = \zeta_2 [\lambda_3 (\alpha_3 \alpha_8 - \alpha_4 \alpha_7) - \lambda_2 (\alpha_2 \alpha_8 - \alpha_4 \alpha_6)]$$

$$+ (\zeta_2 \lambda_4 - \zeta_1)(\alpha_2 \alpha_7 - \alpha_3 \alpha_6). \quad (74)$$

$$H_2^* = -\zeta_2[\lambda_1(\alpha_3 \alpha_8 - \alpha_4 \alpha_7) - \lambda_2(\alpha_1 \alpha_8 - \alpha_4 \alpha_5) + \lambda_4(\alpha_1 \alpha_7 - \alpha_3 \alpha_5)] \\ + \zeta_1(\alpha_3 \alpha_8 - \alpha_4 \alpha_7 + \alpha_1 \alpha_7 - \alpha_3 \alpha_5). \quad (75)$$

$$H_3^* = \zeta_2[\lambda_1(\alpha_2 \alpha_8 - \alpha_4 \alpha_6) - \lambda_3(\alpha_1 \alpha_8 - \alpha_4 \alpha_5) + \lambda_4(\alpha_1 \alpha_6 - \alpha_2 \alpha_5)] \\ - \zeta_1(\alpha_2 \alpha_8 - \alpha_4 \alpha_6 + \alpha_1 \alpha_6 - \alpha_2 \alpha_5). \quad (76)$$

$$H_4^* = -\zeta_2[\lambda_1(\alpha_2 \alpha_7 - \alpha_3 \alpha_6) - \lambda_3(\alpha_1 \alpha_7 - \alpha_3 \alpha_5) \\ + \lambda_2(\alpha_1 \alpha_6 - \alpha_2 \alpha_5)] + \zeta_1(\alpha_2 \alpha_7 - \alpha_3 \alpha_6). \quad (77)$$

Solute concentrations c_1 and c_2 in real time may be obtained by numerical inversion. For brevity, solutions when $W_2 < 0$ and/or $W_4 < 0$ are omitted.

Acknowledgements

Support of the National Science Foundation under contract EEC-9209619 is gratefully acknowledged. M. Bai would like to express his appreciation to Dr. J.-C. Roegiers for his encouragement and support, to Dr. F. Civan and Dr. A. Bouhroum for their critical comments and help in providing experimental data.

References

- Bear, J., 1972: *dynamics of Fluids in Porous Media*, American Elsevier, New York.
- Bibby, R., 1981: Mass transport of solutes in dual-porosity media, *Water Resour. Res.* **17**, 1075–1081.
- Bouhroum, A., 1993: Is tailing of breakthrough curves diffusive? theoretical and experimental evaluation, paper 13, *5th Saskatchewan Petroleum Conf.*, Regina, Canada.
- Deans, H. A., 1963: A mathematical model for dispersion in the direction of flow in porous media, *Trans. AIME* **228**, 49–52.
- Coats, K. H. and Smith, B. D., 1964: Dead-end pore volume and dispersion in porous media, *SPEJ* **4**, 73–84.
- Gerke, H. H. and van Genuchten M. T., 1993: A dual-porosity model for simulating the preferential movement of water and solutes in structured porous media, *Water Resour. Res.* **29**, 305–319.
- Harrison, B., Sudicky, E. A. and Cherry, J. A. 1992: Numerical analysis of solute migration through fractured clayey deposits into underlying aquifers, *Water Resour. Res.* **28**, 515–526.
- Huyakorn, P. S. and Pinder, G. F., 1983: *Computational Methods in Subsurface Flow*, Academic Press, New York.
- Imdakm, A. O. and Sahimi, M., 1991: Computer simulation of particle transport processes in flow through porous media, *Chem. Eng.* **46**, 1977–1993.
- Joy, D. M. and Kouwen, N., 1991: Particulate transport in a porous medium under non-linear flow conditions, *J. Hydraulic Res.* **29**, 373–385.
- Joy, D. M., Lennox, W. C. and Kouwen, N., 1993: Stochastic model of particulate transport, *J. Hydraulic Eng.* **119** 846–861.
- Koenders, M. A. and Williams, A. F., 1992: Flow equations of particle fluid mixtures, *Acta Mechanica* **92**, 91–116.
- Leo, C. J. and Booker, J. R., 1993: Boundary element analysis of contaminant transport in fractured porous media, *Int. J. Numer. Anal. Methods Geomech.* **17**, 471–492.

- Mathematical Handbook*, 1979: People's Education Publishing Company [in Chinese] 1398 pp.
- Neretnieks, I. 1993: Solute transport in fractured rock – Applications to radionuclide waste repositories, Bear, J., C.-F. Tsang and G. De Marsily (eds.), *Flow and Contaminant Transport in Fractured Rock*, Academic Press, San Diego, Ca, pp. 39–128.
- Nilson, R. H. and Lie, K. H., 1990: Double-porosity modeling of oscillatory gas motion and contaminant transport in a fractured porous medium, *Int. J. Numer. Anal. Methods Geomech.* **14**, 565–585.
- Passioura, J. B., 1971: Hydrodynamic dispersion in aggregated media, 1. Theory, *Soil Sci.* **111** 2. Effects of velocity and aggregate size, *Soil Sci.* **111**, 345–351.
- Piquemal, J., 1992: On the modeling of miscible displacements in porous media with stagnant fluid, *Transport in Porous Media* **8**, 243–262.
- Piquemal, J., 1993: On the modeling conditions of miscible displacements in porous media presenting capacitance effects by a dispersion-convection equation for the mobile fluid and a diffusion equation for the stagnant fluid, *Transport in Porous Media* **10**, 271–283.
- Rowe, R. K. and Booker, J. R., 1990: Contaminant migration in a regular two- or three-dimensional fractured network: reactive contaminants, *Int. J. Numer. Anal. Methods Geomech.* **14**, 401–425.
- Sardin, M. and Schweich, D., 1991: Modeling the nonequilibrium transport of linearly interacting solutes in porous media: a review, *Water Resour. Res.* **27**, 2287–2307.
- Stehfest, H., 1970: Algorithm 358 – Numerical inversion of Laplace transforms, *Comm. ACM* **13**, 47–49.
- Sudicky, E. A. and McLaren, R. G., 1992: The Laplace transform Galerkin technique for large-scale simulation of mass transport in discretely fractured porous formations, *Water Resour. Res.* **28**, 499–514.
- Udey, N. and Spanos, T. J. T., 1993: The equations of miscible flow with negligible molecular diffusion, *Transport in Porous Media* **10**, 1–41.